Detailed physical modeling of wildland fire dynamics at field scale - An experimentally informed evaluation

Detailed physical modeling of wildland fire dynamics at field scale - an experimentally informed evaluation

Eric V. Mueller[a*], Nicholas Skowronski[b], Kenneth Clark[b], Michael R. Gallagher[b], William E. Mell[b], Albert Simeoni[c], Rory M. Hadden[a]

[a]School of Engineering, University of Edinburgh, Edinburgh, UK
e.mueller@ed.ac.uk

[b]USDA Forest Service, Morgantown, WV, New Lisbon, NJ, and Seattle, WA, USA

[c]Worcester Polytechnic Institute, Worcester, MA, USA

[*]Corresponding author

Abstract: Computational Fluid Dynamics (CFD) models are powerful research tools for studying fire dynamics. However, their application to wildland fire scenarios requires evaluation against relevant experimental data. To progress our current understanding of the fidelity of a CFD approach to simulating wildland fire dynamics, a dataset from an experimental fire was used as a test case. First, implications of the level of detail provided to the model, in the form of fuel structure and wind, are evaluated. Second, the predictions of both fire behavior (e.g. spread rate) and the driving combustion processes (e.g. heat flux) are compared to the experiment. It was found that both increasing the detail in canopy fuel structure and implementing turbulent boundary conditions had a minor impact. It was further found that the model reproduced fire behavior in the mid-range of experimental observations and that the representation of local combustion processes was qualitatively consistent. This work demonstrates the promising capabilities of the modeling approach used here, while showing that some of its aspects require further investigation and possibly more development.

Keywords:

wildfires, fire spread, modeling, CFD

1. Introduction

The use of Computational Fluid Dynamics (CFD) models for studying a variety of problems related to fire safety engineering in the built environment is well established. While ongoing model development continues to be a high-priority research area [1], these tools have a history of accepted application. On the other hand, the use of CFD models for studying wildland fires, which can span a large range of scales and involve complex conditions (porous fuels, weather effects, etc.), continues to draw more significant debate within the research community [2]. Therefore, evaluating such models against data from field-scale fires is an important step in understanding the current capabilities of the approach, while also helping to identify mechanistic shortcomings which require additional

model development [2–4].

Some previous studies have compared detailed physics-based fire behavior models to measurements from field-scale experimental fires in grasslands (e.g. [5, 6]), and forested environments [7, 8]. However, these have been based on a limited number of experiments (essentially two campaigns in grasslands, and one in a forest). While these studies are valuable for cross-model comparisons, more are needed at this scale, encompassing a range of fuel and environmental conditions. Moreover, spread rate is typically the main, or only, direct point of comparison, and only the studies of Dupuy et al. [6] and Pimont et al. [8] have investigated model predictions of quantities such as temperature, velocity, and heat flux at field-scale. Such quantities can shed light on whether seemingly accurate predictions of fire behavior are indeed a function of adequate representations of the driving combustion processes.

The work presented here aims to address some of these gaps by using an experimental fire in a forested environment, with well-quantified fuels and fire behavior [9, 10], as a comparison case for a previously established CFD model, the Wildland-urban interface Fire Dynamics Simulator (WFDS) [5, 11]. The objectives are twofold: (1) to begin to explore the relationship between the level of detail used to describe the environment (fuel and weather) and the predicted fire behavior; and (2) to assess the ability of the approach to replicate the fire behavior (defined as the characteristics of the fire, such as spread rate) as well as the underlying processes, as obtained in field measurements. These objectives will bring new insight to the current challenges in the use of physics-based models to describe wildland fire dynamics, both in terms of obtaining the necessary model inputs and in having the proper measurements (or fundamental understanding) to evaluate the outputs.

The first objective speaks to the challenges in setting up the model - particularly given the level of detail which such tools allow (even require). In this study, we investigate the role of increasing detail applied to both the boundary (wind) conditions and vegetation structure. The former is modified by including a stochastic model for turbulent fluctuations at the upwind boundaries, and the latter by modifying the heterogeneity specified in the three-dimensional distribution of canopy fuel density. The effect that these modifications have on predicted fire behavior is then evaluated.

The second objective speaks to the challenges in evaluating model performance against real data. It is often easier to obtain comparison points for descriptors of fire behavior, but it is equally important to understand how various processes lead to this behavior and how well they are captured. Here, we focus on measurements of gas-phase temperature (which gives insight into flame structure), flow at surface level (which is important for capturing convective processes and supplying oxygen to the combustion zone), and radiative heat flux ahead of the front (which can be an important mechanism for fire spread).

2. Methods

2.1 Experimental data

The test case for this modeling investigation was a large-scale (4.25 ha) experimental fire, carried out in 2014. This fire was conducted in a pitch pine (*Pinus rigida*) dominated stand in the Pinelands National Reserve (PNR) of New Jersey, USA. This fire spread as a moderate- to high-intensity surface fire, with localized regions of crown fire. A complete description of the test conditions (fuel structure and environment) and of the fire behavior can be found in Mueller et al. [9]. Measurements of local fire properties, critical for model evaluation as discussed previously, were also made at specific sites within the burn area (sites F1-3 in Fig. 1). Gas-phase temperatures (vertical array of thermocouples), fluid velocities (bi-directional pressure probes), and radiative heat fluxes (thin-skin calorimeters) were measured, and a detailed description and analysis can be found in Mueller et al. [10].

2.2 Numerical approach

The numerical simulations discussed in this paper were carried out using a multiphase formulation for incorporating subgrid-scale thermally-thin fuel (vegetation) within a 3-dimensional CFD domain [12]. In this case, the computational framework used to employ the multiphase approach was WFDS, which is built upon version 9977 of the Fire Dynamics Simulator (FDS) - a well-known CFD model developed for fires in the built environment [13]. Details related to the representation of vegetation through the multiphase approach are available in [5, 11]. The source code for WFDS is available open-source through the USDA Forest Service, with modifications relevant to running these simulations published in Mueller [14]. Using this tool, the results of four simulations are presented here - exploring the effect of turbulent boundary conditions and canopy structure, as described below. One simulation is then selected for a more detailed analysis of the representation of local combustion processes.

The modeling of the turbulent combustion environment followed the standard choices used in FDS. Specifically: the Deardorff model for subgrid turbulence closure, a single-step infinitely fast combustion reaction based on the Eddy Dissipation Concept (EDC), and user-defined global radiative fraction [13]. As this study focused on the aspects of the numerical approach specific to wildland fires, details of these submodels are not discussed further. However, the parameterization of the model related to wildland fire applications is discussed in the following sections. It is acknowledged that many choices made in this step can impact the results, but this is beyond the present scope and the reader is directed to Mueller [14] for a study on this aspect.

2.2.1 Vegetation description

Vegetation input parameters are summarized in Table 1. The forest litter layer was assumed to be comprised only of dead pine needles. Due to difficulty in resolving a shallow

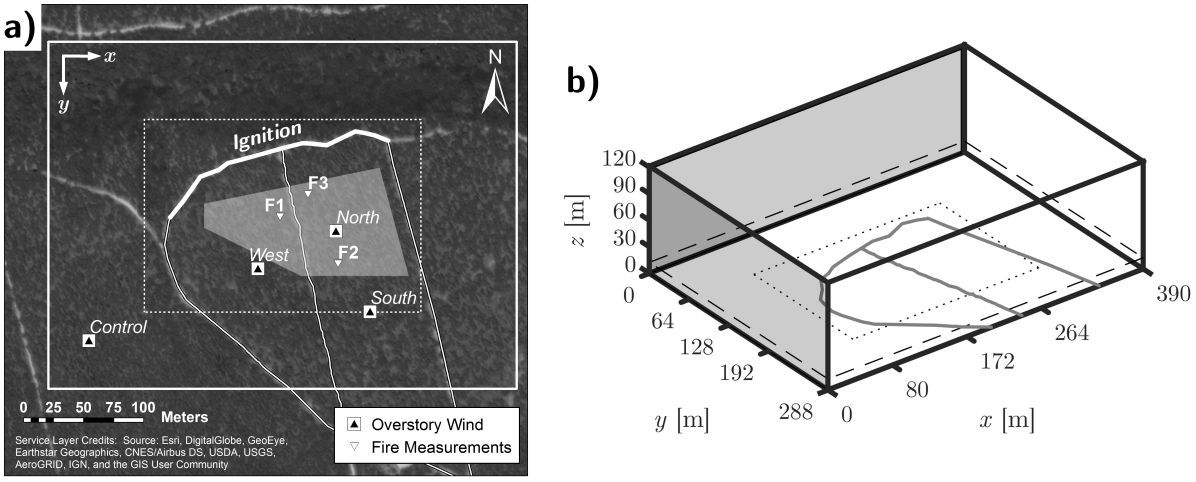

Fig. 1. Numerical domain shown (a) over satellite imagery (as solid line), and (b) in 3-dimensions. The dotted line shows the footprint of the higher-resolution grid. In (a) the detailed measurement sites are marked as triangles and the area used to compute average fuel consumption is shown as a shaded polygon. In (b) the inlet boundaries are shaded gray (x=0 m, y=0 m), and the average canopy height is shown as a dashed line.

litter layer within a large domain, it was treated as a boundary condition with a 1-dimensional heat transfer model and mass, energy, and momentum exchanges occurring at the lowest gas-phase grid cells, following Mell et al. [5]. Thermal decomposition of solid fuel in this layer was modeled with a simple approach, which involved the conversion of moisture to water vapor at a fixed temperature and the conversion of virgin material to gaseous fuel and char (pyrolysis) as a linear function of temperature (e.g. [11]). The shrub and canopy fuel layers were included within the domain. Shrubs were modeled as thin woody fuel (comprised of ¡6 mm diameter particles, grouped into three size classes and the canopy as a mix of live needles and thin woody fuel (comprised of ¡6mm particles and treated as one representative size class) as detailed in Table 1. Thermal decomposition of solid fuel in these layers was modeled with three independent, single-step Arrhenius reactions: one for the conversion of moisture to water vapor, one for the conversion of virgin material to gaseous fuel and char, and one for the surface oxidation of char (e.g. [15]). A representative formula for wood pyrolysate ($C_{3.4}H_{6.2}O_{2.5}$) was also adopted from past work as the gaseous fuel vapor produced by all vegetation types considered [11].

Physical properties of pitch pine needles were obtained from field and laboratory measurements. Woody fuels were prescribed a typical density value for wood, and the surface-to-volume ratio was estimated using a median diameter for the relevant size class. Radiative, char, and soot fractions were based on values used in previous simulations of combustion of vegetation [11]. Average bulk density values for the litter and shrub layers, determined from field sampling, were applied across the entire domain. The layer depths were set, based on measurements, to be 5 cm and 1.0 m, respectively (the value for the

shrub layer was partially constrained by numerical resolution).

Table 1: Input Values for surface-to-volume ratio (σ), bulk density (ρ_b), element density (ρ_e), moisture content on a dry basis (M), radiative fraction (χ_r), char fraction (χ_c), soot yield (χ_s), and gas-phase heat of combustion (ΔH_c). Subscripts refer to live canopy needles (ln), dead litter-layer needles (dn), canopy woody fuels (cw), and fine woody shrub fuels (s). Shrub fuels are subdivided into diameter categories of 0-2 mm ($s1$), 2-4 mm ($s2$), and 4-6 mm ($s3$).

Property	Value	Property	Value	Property	Value
σ_{ln}, σ_{dn}	4661 m^{-1}	σ_{cw}	1333 m^{-1}	$\rho_{b,s1-3}$	0.186 $\mathrm{kg{\cdot}m}^{-3}$
$\rho_{b,ln}$	see Fig. 2	$\rho_{b,cw}$	see Fig. 2	$\rho_{e,s1-3}$	512 $\mathrm{kg{\cdot}m}^{-3}$
$\rho_{e,ln}$	787 $\mathrm{kg{\cdot}m}^{-3}$	$\rho_{e,cw}$	512 $\mathrm{kg{\cdot}m}^{-3}$	M_{s1-3}	60%
M_{ln}	115%	M_{cw}	85%	χ_r	0.35
$\rho_{b,dn}$	20.6 $\mathrm{kg{\cdot}m}^{-3}$	σ_{s1}	4000 m^{-1}	χ_c	0.25
$\rho_{e,dn}$	615 $\mathrm{kg{\cdot}m}^{-3}$	σ_{s2}	1333 m^{-1}	χ_s	0.02
M_{dn}	20%	σ_{s3}	800 m^{-1}	ΔH_c	17 $\mathrm{MJ{\cdot}kg}^{-1}$

Airborne LiDAR measurements were used to derive the 3-dimensional structure of canopy fuels, in the form of spatially varying bulk density [16]. Three approaches were considered in order to assess the impact of canopy fuel structure on fire behavior (see Fig. 2). The first approach applied an average vertical profile for the whole study area to the entire computational domain. The second approach estimated bulk density variation in 1 m vertical layers over a 10 m x 10 m horizontal grid (as in Mueller et al. [9]). The third approach used Tiffs (A Toolbox for LiDAR Data Filtering and Forest Studies) [17] to create a 2-dimensional map of polygons from identified tree crowns. LiDAR data were then spatially aggregated in these polygons, rather than the 10 m x 10 m grid used in the second approach. This produced spatially varying bulk densities with a 0.5 m horizontal resolution and 1.0 m vertical resolution, which was deemed more representative of the forest structure (see Mueller [14] for more detail). The cumulative distribution of bulk density in the canopy (Fig. 2d) shows that the homogeneous canopy retains the same median density as the 10 m grid, while losing the tails of the distribution. In the polygon approach, the concentration of mass into tree crowns serves to broadly increase the bulk density (and likewise introduce inter-crown spaces with no mass).

2.2.2 Boundary conditions

Ambient wind in the experiment was directed from the northwest, with an average of 3.9 $\mathrm{m{\cdot}s}^{-1}$ at 12 m (nominally canopy height). To match this direction, the $x = 0$ and $y = 0$ planes in the numerical domain were treated as fixed velocity boundaries. The vertical profile of inlet velocity was set to follow a typical profile for forest canopies, with a logarithmic profile above the canopy, an inflection point at the canopy surface, and an exponential profile below. The experimental measurements of mean and friction velocity at canopy height were used to parameterize this profile with the appropriate magnitude [14].

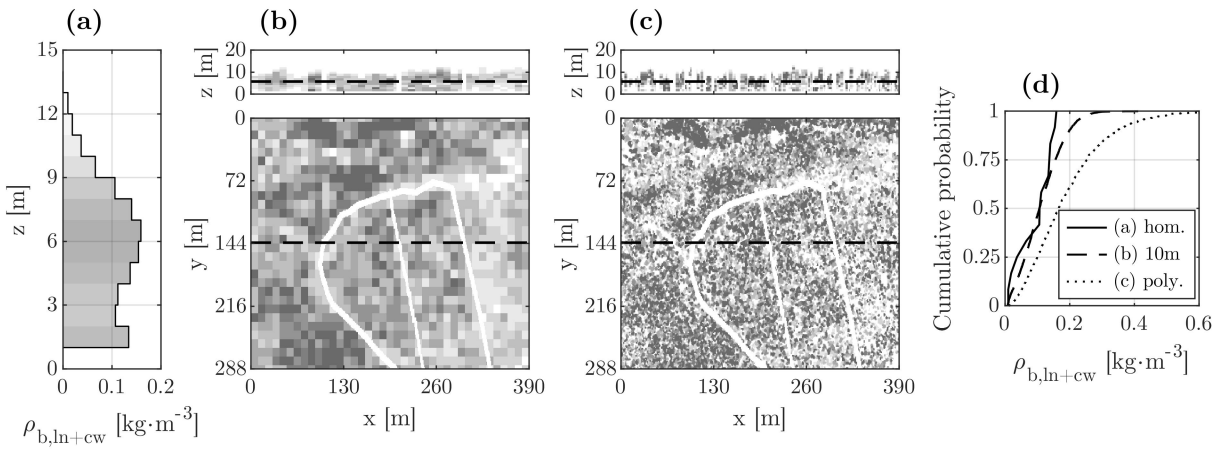

Fig. 2. Comparison of the (a) homogeneous, (b) 10 m x 10 m grid, and (c) polygon distributions canopy bulk density (live needles and thin branches). Section views of the canopy are at $y = 144$ m, plan views at $z = 5.5$ m. As shrub fuels dominate below 1 m, the bulk density within this volume is specified from field sampling values and is not included here. (d) Cumulative density functions of all canopy bulk density values within the burn area (zero values ignored).

A comparison is made here between the specification of a static flow profile and the introduction of turbulent fluctuations in the inlet flow. The latter was accomplished by implementing the so-called Divergence Free Synthetic Eddy Method (DFSEM) [18]. This randomly introduces eddies which are advected through the inlet plane. Their characteristics were obtained from sonic anemometer measurements of the turbulent Reynolds stresses in the ambient wind at canopy height, and are scaled in the vertical direction (see description and verification in Mueller [14]). The remaining lateral boundary conditions were specified as 'open' (free exchange with ambient) [13], and vertical flow was suppressed at the upper boundary to help maintain the horizontal flow. This was needed to help represent the influence of the momentum of the atmosphere above, as the ambient flow tends to deflect upward otherwise. The main region of interest for the fire dynamics here is $O(10)$ m, and the imposed condition is ten times greater in height. Further, due to the ambient wind, the plume in this case is largely advected out of the domain through the open lateral boundaries, where vertical motion is not suppressed. This constraint is therefore considered to have a minimal impact on the fire behavior at the level of the flame front.

Ignition was simulated by activating a line of combustion along the northern edge of the block. This line was progressively extended from east to west to match the progressive drip-torch ignition (which was tracked by GPS).

2.2.3 Computational parameters

The numerical domain covered a volume of 390 m x 288 m x 121.5 m, of which a sub-region of 230 m x 160 m contained the area of actual fire spread (shown in Fig. 1). Note that this domain only allows for spread to be simulated up to the south overstory tower. This helps to reduce the computational cost as the observed fire intensity decreased dramatically after this point [9]. The region of fire spread employed a horizontal grid cell spacing of 0.5 m x 0.5 m, while the surrounding domain used a 1.0 m x 1.0 m spacing. Throughout the entire domain, the vertical resolution was 0.5 m up to a height of 26 m, 1.0 m up to 39 m and 1.5 m thereafter. The radiation solver was discretized over 500 solid angles. This was increased over the default value of 100, following previous suggested resolutions of 500-1000 angles (e.g. [19, 20]) while attempting to manage computational cost. However, these past studies have not focused on spreading line fires, and more work is likely needed to define suitable resolution for wildland fire scenarios. Computations were distributed over 78 CPU cores, with runtimes in the range of 36-44 h for 900 s of simulation time.

3. Results and discussion

3.1 Heterogeneity effects of fuel and wind

The influence on simulated fire behavior due to adjusting canopy heterogeneity and introducing turbulent boundary conditions (DFSEM) is summarized in Table 2. Refining the description of canopy structure had a negligible impact, with the spread rate varying by only 8% of the average across all simulations, and similarly small variations are obtained for fuel consumption in the different layers. The fact that reasonable estimates of fire spread were produced even with a relatively coarse description (homogeneous case), can be traced back to the fact that overall, the canopy was highly dispersed (low ρ_b) compared with the litter and shrub layers. Therefore, the influence of the combustion of this layer is correspondingly reduced. This is in line with the previous suggestion that shrub and litter variability drove the local variations in fire spread observed in the experiment [9], as the simulation assumed uniform fuel structure for these layers, and produced generally steady fire behavior during the period of interest. A study by Pimont et al. [21], using another physics-based model, also found that the influence of detailed canopy structure was only significant for higher fuel loads (high density canopies).

The introduction of turbulence at domain boundaries also had minimal impact on average behavior. However, examination of time-resolved fire progression, determined on a transect on the eastern half of the burn area (Fig. 3), does indicate that the use of DFSEM produces a more steady spread over the duration. The case without DFSEM (S1) initially progressed more rapidly, traversing the first 75 m about 25 s quicker than the other cases, but then slowed and reached 140 m about 60 s after the other cases. This can be linked to the fact that the flow field was more stable (turbulence was produced at the inlet, rather than involving a downstream transition to turbulence, induced by canopy shear). At increasing distances from the inlet, the canopy shear should naturally induce similar

Table 2: Mean (standard deviation) spread rate (R) and mass consumption (Δm) for the different simulations. Spread rate was determined on the transect in Fig. 3, between the ignition and P4. Mass consumption was determined for the litter (l), shrub (s), and canopy (c) fuel layers within the polygon identified in Fig. 1, and was treated on a fuel load basis (mass per unit area).

Name	Description	R [m·s^{-1}]	Δm_l [%]	Δm_s [%]	Δm_c [%]
S1	10m canopy grid; static inlets	0.25 (0.09)	91 (3)	84 (7)	33 (22)
S2	10m canopy grid; DFSEM	0.25 (0.07)	91 (6)	83 (7)	38 (22)
S3	homogenous canopy; DFSEM	0.26 (0.08)	90 (3)	84 (5)	38 (19)
S4	polygon canopy; DFSEM	0.27 (0.08)	92 (4)	84 (7)	37 (25)
EX	experiment	0.19 (0.05)	74 (36)	76 (45)	39 (19)

turbulent characteristics in either case, as indicated by a previous study of canopy flows using WFDS [22]. In the conditions of this moderate- to high-intensity fire, the influence of the buoyant plume likely dominated the generation of turbulence, further reducing the impact of any differences in the downstream development of canopy-induced turbulence between the approaches. Raupach [23] suggested that when the vertical plume velocity outweighs the canopy shear friction velocity (which was the case observed here [14]) the effect of ambient turbulence on the plume is insignificant. Nevertheless, the potential influence of the spatial uniformity (or lack thereof) and turbulent characteristics of the wind field on more marginal burning scenarios will be important to consider in future - for example if considering low-intensity fires or the early stages of fire growth from a local ignition source. Given the similarity between all approaches, however, a single simulation, S2, is chosen for more detailed analysis below.

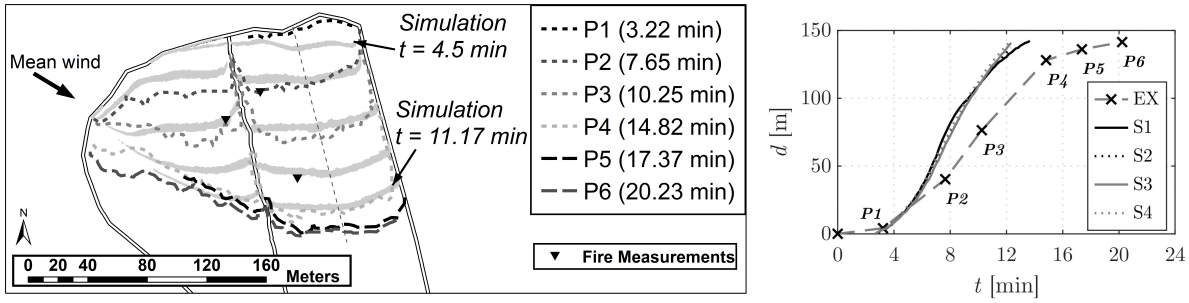

Fig. 3. (left) Snapshots of the surface pyrolysis front in simulation S2, shown every 100 s, along with experiment IR isochrones (P1-6). The transect used to analyze fire spread is shown as a dotted line extending south from the ignition line. (right) Fire front progression along the specified transect. Experimental time is given in minutes from ignition, with simulation times adjusted so the fire location matches at P1.

3.2 Fire progression

The progression of the simulated fire front (extracted as the region of pyrolysis in the litter fuels) is shown for S2 in Fig. 3. The initial progression on the eastern side is not fully parallel to the ignition line, unlike the experiment. This is likely due to uncertainty in the replication of the ignition procedure (timing and intensity). However, the fire front isochrones tend towards the same geometry as the experiment by about 6 min after simulated ignition. Thus, while capturing the ignition pattern is critical, small uncertainties do not appear to impact the behavior at long times after ignition.

Overall, there is a tendency for over-prediction of the mean spread rate in the simulation (Table 2, Fig. 3), exceeding the experimental average by ∼30%. This puts the simulated behavior in the range of observed spread rate for typical high intensity surface fires with some canopy involvement in this ecosystem (e.g. [9, 24]). It is lower, however, than the highest local spread rate observed in the experiment (0.4 $\mathrm{m{\cdot}s^{-1}}$ during full canopy involvement at F2 [10]). Indeed, the mean simulated spread rate is a good match to certain periods of the experiment (relative error <10% during P2-P3). In both the experiment and simulations, the western side of the fire front spreads slower than the eastern side. This can be attributed to the ambient wind direction (Fig. 3). The wind flows from the northwest, almost parallel to the orientation of the developing flank, and is drawn into the main front. This parallel flow both limits the ability of the flank to entrain air and prevents bursts of convective heating perpendicular to the front. However, the simulated fire front also starts to extinguish at the very western edge. This may be associated with a known issue in capturing flanking fire behavior for more coarsely resolved cases [5], but this region did not contain fire measurement sites and so the remaining comparisons are valid.

3.3 Local fire dynamics

Using the contours of the surface pyrolysis front (Fig. 3), simulated local spread rates of 0.37 $\mathrm{m{\cdot}s^{-1}}$, 0.3 $\mathrm{m{\cdot}s^{-1}}$ and 0.32 $\mathrm{m{\cdot}s^{-1}}$ were found for sites F1, F2, and F3, respectively. These fall between the local estimates of 0.19 $\mathrm{m{\cdot}s^{-1}}$, 0.4 $\mathrm{m{\cdot}s^{-1}}$ and 0.15 $\mathrm{m{\cdot}s^{-1}}$ at the respective experimental sites. Thus the local simulated processes should be indicative of behavior between a surface fire (observed in the experiment at F1 and F3) and localized crown fire (observed in the experiment at F2).

3.3.1 Gas-phase temperatures

A comparison of the flaming characteristics observed at the lowest and highest thermocouples on the array is given in Table 3. Simulated temperatures within the shrub layer (0.6 m) fall between 954–1062 °C, a narrower range than the experimental observations (814–1017 °C) and shifted slightly higher. However, the experiments are not a direct measure of gas-phase temperature, and depending on the surrounding environment, the thermocouples may be on the order of 10% lower than the actual value [25].

Presence of the flame (and thus residence time and intermittency during the residence) was

Table 3: Flaming characteristics at the three sites. Measurements are peak gas-phase temperature (T_{max}), residence time (t_r), and flame intermittency (Λ).

Site	h [m]	T_{max} [°C]		t_r [s]		Λ [-]	
		EX	S2	EX	S2	EX	S2
F1	0.6	947	1062	19.8	26.4	0.80	1.00
	2.4	708	1028	17.7	20.5	0.67	0.32
F2	0.6	814	954	31.3	18.1	0.79	0.95
	2.4	875	844	29.5	15.2	0.77	0.53
F3	0.6	1017	965	27.8	18.0	0.88	0.97
	2.4	664	774	22.2	15.5	0.41	0.60

determined based on a 300 °C threshold. The simulated residence times in the shrub layer are relatively consistent between the sites, and resemble the roughly 20–30 s experimental range. The residence times at the uppermost thermocouples are not as prolonged, particularly at the crown fire site (F2), where it is 50% the experimental value. The simulated flame intermittency also tends to be lower at the upper thermocouple, and taken together the duration of flame contact in the lower canopy is less substantial in the model. It should be noted, however, that intermittency and the choice of a temperature threshold will introduce uncertainty in estimated flame contact.

Despite this under-prediction, the simulations over-predicted canopy fuel consumption in the lower layers (see [14] for more details). This demonstrates a tendency of the canopy fuel to be consumed too easily (though the effect of this combustion on overall fire behavior is small, as discussed above). Outside of the arguably crude representation of the forest canopy in this simulation, the physics of the drying and combustion of live fuels are still poorly understood [26] and are not differentiated in the model (except through increased moisture). Nevertheless, this points to an area for investigation and continued model development, particularly for applications which are focused on live forest canopies.

The simulated effect of entrainment and mixing on flame and plume temperatures was investigated on a 2-D plane perpendicular to the fire font. Using a moving reference frame, the average centerline temperature (greatest temperature at a given height) was obtained for a 400 s period of quasi-steady spread. This is plotted against scaled distance in Fig. 4. Due to tilting by ambient wind, distance traveled by smoke (s) was estimated using mean velocity vectors at the plume centerline. Previously, temperature rise above axisymmetric fires has been scaled by heat release rate [27], and in the case of line fires this is typically 'heat release rate per unit length' (analogous to fireline intensity) raised to the two-thirds power ($Q_l^{2/3}$) [28, 29]. For S2 this was estimated locally as 6.5 MW·m^{-1}, based on the integral of energy release on the same 2-D plane as the temperature and velocity fields.

Axisymmetric fires have been found to produce a constant temperature region ($\eta = 0$) in the continuous flame, an inversely proportional decay in the intermittent flame region ($\eta =$ -1), and a steeper decay in the plume ($\eta =$ -5/3) [27]. However, it has been suggested that for line fires the decay will remain inversely proportional in the plume region (potentially

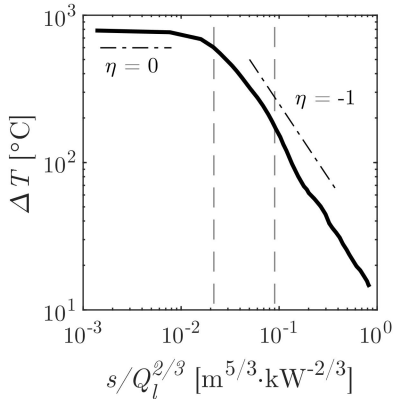

Fig. 4. Average maximum temperature rise against scaled distance for S2. Estimates of the continuous, intermittent, and plume regions are separated by vertical dashed lines. Typical exponents for the temperature relationship are given (η, dot-dash lines).

up to 6 flame heights) [28]. This was attributed to the wide linear plume restricting lateral entrainment to the center, closer to the source. Here, the temperature rise follows a similar relationship, indicating the model is able to reproduce reasonable temperature fields at both a local and large scale.

3.4 Flow

A comparison of the influence of the fire on horizontal flow, perpendicular to the front at $z = 1.2$ m, is given for sites F1 and F2 in Fig. 5. The downstream effect of entrainment is visible, with a small (typically <3 m·s^{-1}) but largely negative flow (from the south, counter to ambient wind) establishing in both the experiment and simulation. This reversal is first observed in the experimental data at 240 s and 360 s before the fire arrival at F1 and F2, respectively. An estimation from the progression puts the fireline 45 m and 80 m away at these times. In the simulation the reversal times are roughly 160 s and 260 s, and the distances are 50 m and 90 m, respectively. Given the uncertainty in the distance, the simulated downstream influence of the fire is quite consistent with the experiment. It should also be noted that the onset of the flow reversal at F1 is close to the time of ignition and the early stages of fire growth in this segment of the block, and this distance might be in greater agreement with that at F2 if the fire had established much further away.

Upwind entrainment effects have been observed in previous experiments, relatively close to the fire front in grass fires (exact distance unknown) [30, 31], and up to a distance of at least 150 m from the plume in a mass fire experiment [32]. The fire intensities (plume buoyancy) and ambient wind speeds may be considerably different in these cases, but limited quantitative information is available for comparison on these large-scale fire-induced upwind flow reversals. In a numerical study using FDS, dependence of flow reversal distance on wind and fire intensity was demonstrated [33]. For wind speeds and

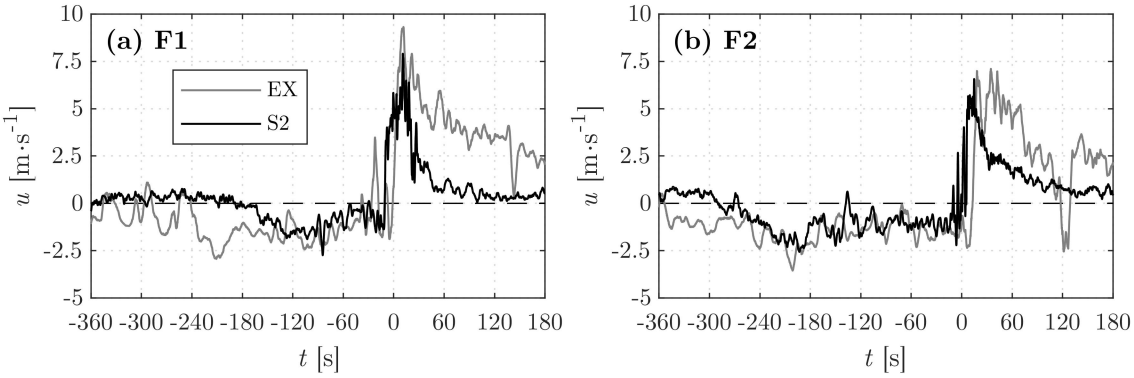

Fig. 5. Horizontal velocity (streamwise direction) for sites (a) F1 and (b) F2. Positive values are in the direction of fire spread. Curves represent a 1-second moving average. Time scales are adjusted to the arrival of the fire at the primary tower ($t = 0$).

intensities similar to those found here, a distance of 70 m was suggested, which is comparable to both the experimental and simulation results. However, a 2-dimensional approach was used, which may over-predict such effects [34], and this phenomena warrants further investigation. Along with the relative strength of ambient wind and buoyant flow, differences in past studies may also be linked to terrain and vegetation features which can serve to enhance sheltering in certain situations.

With arrival and passage of the fire front, the flow quickly reverses to match the direction of fire spread and ambient wind, as in the experiments. The simulated velocities reach instantaneous maxima (25 Hz sampling) of 8.9 and 7.9 m·s^{-1} for F1 and F2, respectively. These are lower than the instantaneous experimental maxima (50 Hz sampling) by 40-45% (16.2 m·s^{-1} and 13.1 m·s^{-1}). A 1-second moving average, however, shows a better agreement with the experiment (Fig. 5). Thus the dominant flow trends are replicated, and understanding potential discrepancies in the higher frequency peaks may require more sensitive instrumentation [10]. Following the peak, the simulated horizontal velocity decays following a similar trend to the experiment, but with much lower magnitudes and without the tendency for a strong persistent fire-induced flow well after the passage of the front, as exhibited in the experiments.

This discrepancy can be related to a poor representation of the removal of vegetation in the wake of the fire. Specifically, the drag of a given vegetation class is constant in a model cell unless fully converted to ash. There is no drag reduction considered for partial consumption in a cell, nor is there vegetation breakage in strong gusts, which was observed experimentally in the wake of the fire, and will contribute to drag reduction. It may also be that buoyancy from residual heat, interacting with the downdraft of ambient air typical in the wake of the fire, can generate vortical structures which can enhance horizontal flow [35]. Regardless, this strong draft after the front is important for prolonged smoldering (and thus understanding fire emissions), as well as being particularly key for understanding the mechanism for the generation of firebrands.

3.5 Radiative heat flux

Estimates of incident radiative flux, facing the fire front at $z = 1.1$ m, are shown for F1 and F2 in Fig. 6. While six sensors were located at each site, the experiment revealed the responses to be largely the same, when corrected for different view angles, owing to the integral nature of the measurement at a given location [10]. Therefore a single representative measurement is discussed here. The simulation shows less of a response prior to arrival in both cases, most significantly at F2 (where large fluxes were observed experimentally due to the occurrence of local crown fire behavior). For example, at 5 m the simulated flux is only 36% and 15% of the measured value for F1 and F2, respectively. The signals increase rapidly as the fire approaches, with the arrival at the respective sites ($d = 2$ m) giving simulated flux values 20 kW·m^{-2} and 19 kW·m^{-2} at F1 and F2, and arrival at the sensor ($d = 0$ m) giving ∼60 kW·m^{-2} in both cases.

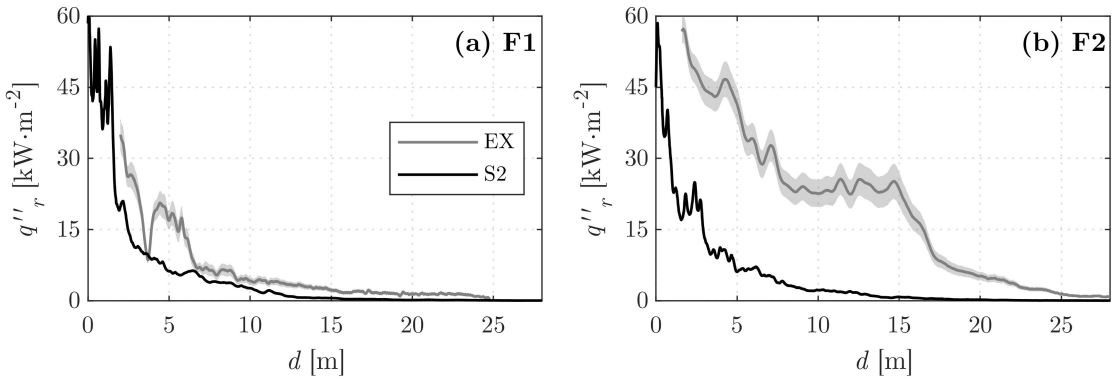

Fig. 6. Incident radiative heat flux (q''_r) at sites (a) F1 and (b) F2 at z = 1.1 m. Distance (d) estimated from estimated from local spread rate. Shaded area represents estimated experimental uncertainty [10].

As the fire front passes, the peak simulated incident radiative heat flux was 105 kW·m^{-2} and 87 kW·m^{-2} for F1 and F2, respectively, at a height of z = 1.1 m. At z = 0.9 m, these values are 157 kW·m^{-2} and 136 kW·m^{-2}. These peak values, close to the shrub layer, are generally consistent with previously reported ranges for brush fires, but are below that of crown fires [36]. This places the peaks of the simulation in a reasonable range, as full crown consumption was not simulated and such high values are not expected. Therefore thermal radiation close to the fire appears more accurately represented.

As for the discrepancy in long-distance values, Hostikka et al. [19] used FDS to study WUI fire scenarios and showed radiative fluxes of ∼25 kW·m^{-2} at 10 m from a 6 MW·m^{-1} fire. This is more comparable to the values measured in the experiment at F2, but there the local fire intensity was estimated to exceed 21 MW·m^{-1} [10]. However, they achieved this intensity with a fixed flow rate from a burner for which the flame geometry may differ from a crown fire and direct comparison is non-trivial. Mell et al. [11] used WFDS to accurately simulate radiative fluxes from a single tree crown in laboratory studies, though these were

measured at maximum distance of 3 m. Further, previous studies focused on radiative transfer across open spaces, while this study considers radiation at significant distances within the fuel layer, where uncertainty in the vegetation extinction coefficient may play a role. The extinction length is determined by the vegetation density and element size (defined as $4\rho_e/\sigma\rho_b$), and the numerical grid size should be smaller to adequately capture radiative absorption [4]. In this work, it is smallest for the thin ($s1$) fuels in the shrub layer (see Table 1), with a value of ~ 2.75 m. The 0.5 m grid resolution should thus be sufficient, but this may be an area for continued investigation. As mentioned previously, the angular resolution of the radiative transport equation was less than the 1000 angles suggested for 3-dimensional simulations by Hostikka et al. [19]. However, the degree of difference they demonstrated between 100 and 1000 angles does not appear sufficient to explain the discrepancy here. In addition to investigating the influence of grid and angular resolution on radiative transport, future work should also be directed at evaluating the use of a conserved global radiative fraction in WFDS and potential sensitivity to its value.

It has been suggested that only the short distance radiation is key in driving fire spread and that fuel may reach thermal equilibrium further away as a result of lower fluxes and environments conducive to convective cooling [37]. This is especially true for thin fuels, which can cool more efficiently [26], and these are generally accepted to play the main role in fire spread. This can explain why spread rates similar to the experiments are achieved despite the under-prediction of long distance radiative fluxes. However, if the model is to be used for applications beyond fire spread, such as studying the thermal impact on tree boles or ignition of thick fuels related to the WUI, this problem must be examined in future work.

4. Conclusions

The ability of a CFD model to represent wildland fire dynamics, both at a plot scale and in terms of the locally driving processes around the flame front, was evaluated by testing the model against data collected in a field-scale experiment. The findings are as follows:

- the modeling approach was able to reproduce fire behavior characteristic of a high intensity surface fire with some canopy involvement, which fell within the experimentally observed range;
- increasing refinements of the description of 3D canopy fuel structure had negligible impact on simulation results, and the inclusion of turbulent boundary conditions had only a minor impact (though this must be considered in the specific context of canopy densities and wind conditions);
- the local processes related to the fire spread (peak temperature rise, fire residence time, peak heat flux, etc.) were qualitatively similar, however, certain discrepancies (fire-induced draft, long range radiative flux) were identified which point to areas where continued investigation is necessary.

This type of modeling approach has been shown previously to successfully describe general trends in fire behavior. However, it is also possible to tune model inputs to more closely match an observation (as is discussed extensively in Mueller [14]). Thus, a main aim here is not to perfectly match a particular feature, but rather (given reasonable reproduction of fire behavior) to assess how well underlying combustion processes are represented.

While the identified discrepancies highlight potential limitations to the current application space for these types of models, they also demonstrate a strength of the approach. Through this work, we are able to identify focus areas where the current understanding of the relevant behaviors is insufficient. This provides a driver not only for continued model development but also renewed experimental efforts to effectively focus on quantifying these behaviors.

5. Acknowledgments

The authors wish to acknowledge the funding support provided through United States Department of Interior Joint Fire Science Program Award #12-1-03-11, as well as the integral support of the New Jersey Forest Fire Service.

6. References

[1] A. Brown, M. Bruns, et al., Proceedings of the first workshop organized by the IAFSS Working Group on Measurement and Computation of Fire Phenomena (MaCFP), Fire Saf. J. 101 (2018) 1–17. doi:10.1016/j.firesaf.2018.08.009.

[2] M. E. Alexander and M. G. Cruz, Are the applications of wildland fire behaviour models getting ahead of their evaluation again?, Environ. Model. Softw. 41 (2013) 65–71. doi:10.1016/j.envsoft.2012.11.001.

[3] W. E. Mell, S. L. Manzello, et al., The wildland–urban interface fire problem–current approaches and research needs, Int. J. Wildl. Fire 19 (2) (2010) 238–251. doi:10.1071/WF07131.

[4] D. Morvan, Physical phenomena and length scales governing the behaviour of wildfires: A case for physical modelling, Fire Technol. 47 (2) (2011) 437–460.

[5] W. Mell, M. A. Jenkins, et al., A physics-based approach to modelling grassland fires, Int. J. Wildl. Fire 16 (1) (2007) 1–22. doi:10.1071/WF06002.

[6] J.-L. Dupuy, F. Pimont, et al., FIRETEC evaluation against the FireFlux experiment: preliminary results, in: Adv. For. Fire Res. - Proc. 7th Int. Conf. For. Fire Res., University of Coimbra: Coimbra, Portugal, 2014, pp. 261–274.

[7] R. R. Linn, K. Anderson, et al., Incorporating field wind data into FIRETEC simulations of the International Crown Fire Modeling Experiment (ICFME): preliminary lessons learned, Can. J. For. Res. 42 (5) (2012) 879–898.

[8] F. Pimont, J.-L. Dupuy, and R. R. Linn, Fire effects on the physical environment in the WUI using FIRETEC, in: Adv. For. Fire Res. - Proc. 7th Int. Conf. For. Fire Res., University of Coimbra: Coimbra, Portugal, 2014.

[9] E. V. Mueller, N. Skowronski, et al., Utilization of remote sensing techniques for the quantification of fire behavior in two pine stands, Fire Saf. J. 91 (2017) 845–854. doi:10.1016/j.firesaf.2017.03.076.

[10] E. V. Mueller, N. Skowronski, et al., Local measurements of wildland fire dynamics in a field-scale experiment, Combust. Flame 194 (2018) 452–463.

[11] W. Mell, A. Maranghides, et al., Numerical simulation and experiments of burning douglas fir trees, Combust. Flame 156 (10) (2009) 2023–2041.

[12] A. M. Grishin, Mathematical modeling of forest fires and new methods of fighting them, Publishing house of the Tomsk State University, Tomsk, Russia, 1997.

[13] K. McGrattan, S. Hostikka, et al., Fire dynamics simulator (version 6), technical reference guide, Tech. rep., Gaithersburg, Maryland (2013).

[14] E. V. Mueller, Examination of the underlying physics in a detailed wildland fire behavior model through field-scale experimentation, Ph.D. thesis, University of Edinburgh (2016).

[15] D. Morvan, G. Accary, et al., A 3D physical model to study the behavior of vegetation fires at laboratory scale, Fire Saf. J. 101 (2018) 39–52. doi:10.1016/j.firesaf.2018.08.011.

[16] N. S. Skowronski, K. L. Clark, et al., Three-dimensional canopy fuel loading predicted using upward and downward sensing LiDAR systems, Remote Sens. Environ. 115 (2) (2011) 703–714. doi:10.1016/j.rse.2010.10.012.

[17] Q. Chen, Airborne lidar data processing and information extraction, Photogramm. Eng. Remote Sensing 73 (2) (2007) 109.

[18] R. Poletto, T. Craft, and A. Revell, A new divergence free synthetic eddy method for the reproduction of inlet flow conditions for LES, Flow, Turbul. Combust. 91 (3) (2013) 519–539. doi:10.1007/s10494-013-9488-2.

[19] S. Hostikka, J. Mangs, and E. Mikkola, Comparison of two and three dimensional simulations of fires at wildland urban interface, Fire Saf. Sci. 9 (2008) 1353–1364.

[20] C. H. Lin, Y. M. Ferng, and W. S. Hsu, Investigating the effect of computational grid sizes on the predicted characteristics of thermal radiation for a fire, Appl. Therm. Eng. 29 (11–12) (2009) 2243–2250. doi:10.1016/j.applthermaleng.2008.11.010.

[21] F. Pimont, J.-L. Dupuy, et al., Impacts of tree canopy structure on wind flows and fire propagation simulated with FIRETEC, Ann. For. Sci. 68 (3) (2011) 523–530.

[22] E. V. Mueller, W. Mell, and A. Simeoni, Large eddy simulation of forest canopy flow for wildland fire modeling, Can. J. For. Res. 44 (12) (2014) 1534–1544. doi:10.1139/cjfr-2014-0184.

[23] M. R. Raupach, Similarity analysis of the interaction of bushfire plumes with ambient winds, Math. Comput. Model. 13 (12) (1990) 113–121.

[24] J. C. Thomas, E. V. Mueller, et al., Investigation of firebrand generation from an experimental fire: Development of a reliable data collection methodology, Fire Saf. J. 91 (2017) 864–871. doi:10.1016/j.firesaf.2017.04.002.

[25] X. Silvani and F. Morandini, Fire spread experiments in the field: Temperature and heat fluxes measurements, Fire Saf. J. 44 (2) (2009) 279–285.

[26] M. A. Finney, J. D. Cohen, et al., On the need for a theory of wildland fire spread, Int. J. Wildl. Fire 22 (1) (2013) 25–36. doi:10.1071/WF11117.

[27] B. J. McCaffrey, Purely buoyant diffusion flames: some experimental results, Tech. rep., Washington, DC (1979).

[28] L.-M. Yuan and G. Cox, An experimental study of some line fires, Fire Saf. J. 27 (2) (1996) 123–139.

[29] J. G. Quintiere and B. S. Grove, A unified analysis for fire plumes, Symp. Combust. 27 (2) (1998) 2757–2766.

[30] C. B. Clements, S. Zhong, et al., Observing the dynamics of wildland grass fires: FireFlux-a field validation experiment, Bull. Am. Meteorol. Soc. 88 (9) (2007) 1369–1382.

[31] C. B. Clements and D. Seto, Observations of fire–atmosphere interactions and near-surface heat transport on a slope, Boundary-Layer Meteorol. 154 (3) (2015) 409–426.

[32] C. M. Countryman and T. G. Storey, Project Flambeau... an investigation of mass fire (1964-1967): final report, Tech. rep., Berkeley, California (1969).

[33] R. Roxburgh and G. Rein, Study of wildfire in-draft flows for counter fire operations, WIT Trans. Ecol. Environ. 119 (2008) 13–22.

[34] R. R. Linn, J. M. Canfield, et al., Using periodic line fires to gain a new perspective on multi-dimensional aspects of forward fire spread, Agric. For. Meteorol. 157 (2012) 60–76.

[35] B. E. Potter, Atmospheric interactions with wildland fire behaviour–II. Plume and vortex dynamics, Int. J. Wildl. Fire 21 (7) (2012) 802–817.

[36] D. Frankman, B. W. Webb, et al., Measurements of convective and radiative heating in wildland fires, Int. J. Wildl. Fire 22 (2) (2013) 157–167.

[37] P. G. Baines, Physical mechanisms for the propagation of surface fires, Math. Comput. Model. 13 (12) (1990) 83–94.

Figure captions

Fig. 1. Numerical domain shown (a) over satellite imagery (as solid line), and (b) in 3-dimensions. The dotted line shows the footprint of the higher-resolution grid. In (a) the detailed measurement sites are marked as triangles and the area used to compute average fuel consumption is shown as a shaded polygon. In (b) the inlet boundaries are shaded gray (x=0 m, y=0 m), and the average canopy height is shown as a dashed line.

Fig. 2. Comparison of the (a) homogeneous, (b) 10 m x 10 m grid, and (c) polygon distributions canopy bulk density (live needles and thin branches). Section views of the canopy are at $y = 144$ m, plan views at $z = 5.5$ m. As shrub fuels dominate below 1 m, the bulk density within this volume is specified from field sampling values and is not included here. (d) Cumulative density functions of all canopy bulk density values within the burn area (zero values ignored).

Fig. 3. (left) Snapshots of the surface pyrolysis front in simulation S2, shown every 100 s, along with experiment IR isochrones (P1-6). The transect used to analyze fire spread is shown as a dotted line extending south from the ignition line. (right) Fire front progression along the specified transect. Experimental time is given in minutes from ignition, with simulation times adjusted so the fire location matches at P1.

Fig. 4. Average maximum temperature rise against scaled distance for S2. Estimates of the continuous, intermittent, and plume regions are separated by vertical dashed lines. Typical exponents for the temperature relationship are given (η, dot-dash lines).

Fig. 5. Horizontal velocity (streamwise direction) for sites (a) F1 and (b) F2. Positive values are in the direction of fire spread. Curves represent a 1-second moving average. Time scales are adjusted to the arrival of the fire at the primary tower ($t = 0$).

Fig. 6. Incident radiative heat flux (q_r'') at sites (a) F1 and (b) F2 at z = 1.1 m. Distance (d) estimated from estimated from local spread rate. Shaded area represents estimated experimental uncertainty [10].

Highlights:

- Predictions of fire behavior were within the range of experiment observations
- Minimal effect of canopy structure or ambient turbulence was found
- Predictions of combustion processes were largely qualitatively consistent
- Certain identified discrepancies provided a basis for recommend future research